Repair wind fi eld in oil contaminated areas with SAR images

Article *in* Chinese Journal of Oceanology and Limnology · March 2015

DOI: 10.1007/s00343-015-3242-7

1 author:

Jie Guo
Chinese Academy of Sciences
20 PUBLICATIONS **112** CITATIONS

SEE PROFILE

Available online at www.sciencedirect.com

ScienceDirect

Aquatic Procedia 3 (2015) 103 – 111

Aquatic Procedia

www.elsevier.com/locate/procedia

International Oil Spill Response Technical Seminar

Repair Wind Field of Oil Spill Regional Using SAR Data

Jie Guo[a,*], Yijun He[b], Xiao Long[c],Chawei Hou[d],Xin Liu[a]

[a] *Yantai Institute of Coastal Zone Research, Chinese Academy of Sciences. 17 Chunhui Road, Laishan District, Yantai, China*
[b] *Nanjing University of Information Science & Technology , School of Marine Sciences,219 Ningliu Road, Nanjing, China*
[c] *Key Laboratory of Arid Climate Change and Reducing Disaster of Gansu Province, College of Atmospheric Sciences, Lanzhou*
[d] *Yantai Marine Environmental Monitoring Central Station,SOA*

Abstract

In this paper, we compared the normalized radar cross section (NRCS) of the synthetic aperture radar in the cases of oil spill and clean sea areas with image samples and determined their thresholds of the NRCS of SAR. we used the NRCS of clean water from the adjacent patches spill area to replace NRCS of oil spill area and retrieval wind field by CMOD5.N and comparison of wind velocity mending of oil spill with Model data the root mean square of wind speed and wind direction inversion are 0.89m/s and 20.26°satisfactory results, respectively. Therefore, after the occurrence not large scale oil spill, the real wind field could be restored by this method.

Peer-review under responsibility of China Offshore Environmental Services Ltd

Keywords: oil spill; NRCS; SAR; wind speed; wind direction

1. Introduction

A wind vector of sea surface is a physical parameter important for understanding atmospheric dynamics, air-sea interactions, and climate. Synthetic aperture radar (SAR) is an active microwave sensor that works all-weather day-and-night in high spatial resolution, which makes it essential for wind velocity inversion, and for monitoring oil spills, biogenic slicks etc. The sea surface roughness responsible for SAR backscatter is produced primarily by capillary and small gravity waves generated by local winds (Brekke and Solberg, 2005). The damping of these waves by oil spills and biogenic slicks appears as dark features in the SAR image (Brekke and Solberg, 2005). The occurrence of an oil spill and biogenic slicks affects the normalized radar cross section (NRCS) of SAR, which would lead to a decrease in the precision of the wind field retrieval. However, oil spill detection in SAR images is

* Corresponding author. Jie Guo Tel.: +86-0535-2109192; fax: +86-0535-2109192
*E-mail address:*jguo@yic.ac.cn

Peer-review under responsibility of China Offshore Environmental Services Ltd
doi:10.1016/j.aqpro.2015.02.233

not an easy task. Other physical phenomena can also generate dark areas and SAR images are affected by multiplicative noise known as speckle (Brekke and Solberg, 2005). Dark areas not related to oil spills are said to be look-alike. Phenomena that give rise to the look-alike include biogenic films, low-wind areas, areas of wind-shadow near coasts, rain cells, currents, up-welling zones, internal waves, and oceanic or atmospheric fronts (Brekke and Solberg, 2005).

Oil spill detection in SAR image can be divided into three phases. They are dark area detection (Solberg and Theophilopoulos, 1997; Espedal and Wahl, 1999; del Frate et al., 2000; Espedal and Johannessen, 2000; Fiscella et al., 2000; Topouzelis et al., 2003), features extraction (Solberg et al., 1999; Brekke and Solberg, 2005; Keramitsoglou et al., 2005; Karathanassi et al., 2006), and oil spill/look-alike classification (Fiscella et al., 2000; del Frate et al., 2000; Keramitsoglou et al., 2006; Topouzelis et al., 2009). Dark area detection algorithms are based generally on filtering techniques accomplished on multi-look single-polarization SAR data (Migliaccio et al., 2009). The use of dual-polarized SAR sensors for oil spill observation is operationally important too. In these studies, dual-polarized SAR measurements were used to enhance oil spill observation. The co-polarized phase difference was modelled and used to characterize the scattering return from oil spills (Migliaccio et al., 2009; Schuler et al., 1993). In the paper, Migliaccio et al. (2009) showed that fully polarimetric features could assist in distinguishing between oil spills.

Ocean surface wind retrieval from conventional single-polarization SAR backscatter measurements is achieved by using various geophysical model functions (GMFs) for X-, C-, and L-band SAR. Specifically, for C-band, the commonly used GMFs are CMOD4 (Stoffelen and Anderson, 1997), CMOD_IFR2 (Quilfen et al., 1998), and CMOD5.n (Hersbach, 2010). Single-frequency (C- or L-band) and single-polarization (VV or HH) SAR systems, such as ENVISAT ASAR (advanced synthetic aperture radar) and COSMO data, have been used to retrieve ocean surface wind speeds with various GMFs and polarization radio (PR) models (Zhang et al., 2012). In this paper, wind fields are retrieved of ASAR data by CMOD5.n and mark oil spill areas, through backscatter coefficient weighted average of the adjacent clean sea area make up the oil spill areas. This work could improve the accuracy of assessment to a real wind field to medium-scale and small-scale (Feng S Z et al., 2003) and provide data support for identification and monitoring of disastrous events such as oil spills areas in maritime.

2. Data and Methods

2.1. Data and study area

One modes of ENVISAT-ASAR data are used in this study: wide swath mode (WSM) (Time: 2011-06-11; Polarization mode: VV; Spatial resolution: 150*150m; Band: C; Watch width: >400km). We analyzed the influence of oil spill on the NRCS, and wind velocity inversion with ENVISAT ASAR data in CMOD5.n.

ENVISAT satellite is one of a series of the Earth observation satellite launched on March 1, 2002, the largest environmental satellite of the Europe bearing 10 devices of which four were improved ones including ERS-1/2, and the heaviest one was ASAR. The ASAR was able to generate high-resolution images on various areas. As a continuation of ERS-1/2 SAR satellite, Envisat-1 was used specifically to continuously monitor the Earth's environments at the surface and in the atmosphere for geo-mapping, resource exploration, weather broadcast, and disaster warning. After her commission for 10 years, the satellite lost communication with the Earth on 8 April 2012. Featured with high resolution, the Envisat-ASAR data could catch the incidence of oil spill on its track. Therefore, SAR plays an important role in recording marine disaster events, such as oil spill etc.

The case area for oil spill was in the Bohai Sea (37°–42°N, 117°–121°E) (Guo et al., 2013) (Fig. 1). We compared the changes caused by oil spill on the NRCS using ENVISAT ASAR data, which can be used to analyze

the effects of oil spill on the retrieval of wind speed data. The data for wind field inversion were the Advanced Scaterometer (ASCAT) data; and the Weather Research and Forecasting (WRF) model was deployed as the auxiliary.

The ASCAT is one of the instruments that carried on-board Meteorological Operational (MetOp) polar satellites launched by the European Space Agency (ESR) and operated by the European organization for the exploitation of Meteorological Satellites (EUMETSAT). ASCAT was launched on 19 October 2006 in C band in frequency at 5.255GHz. The wind products are distributed in two resolutions at 50 km in 25-km grid and at 25 km in 12.5-km grid. Both are available as regional EUMETSAT Advanced Retransmission Service (EARS) products in ~30 interval of sensing and as global OSISAF products in sensing frequency of 2.5–3 h. In this paper, the 25-km daily resolution product in 12.5-km grid data (daily average) was used.

The wind data used are the output of the WRF model with Advanced Research WRF (ARW) in dynamic core version 3.3.1 (Skamarock and Klemp, 2008). WRF is a mesoscalenon-hydrostatic modeling system to a limited-area, and could do terrain tracking, which can be used for simulations from a large-eddy to a global scale.

The latest C-band geophysical model function (GMF) CMOD5 was developed by European Centre for Medium-Range Weather Forecasts (ECMWF) and KNMI for use with the ERS and ASCAT scatterometers. It has been developed using advanced empirical methods, ECMWF model winds that tied to buoy measurement data, and measurements in extreme wind conditions (e.g., hurricanes) from the unique Imaging Wind and Rain Airborne Profiler (IWRAP) instrument aircraft campaigns.

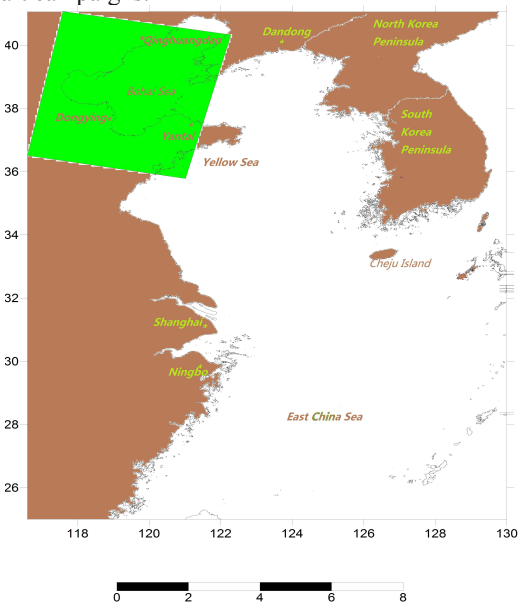

Fig.1. Case study areas: oil-spill area in Bohai Sea (rectangular)

2.2. SAR image samples analysis Method

We used ENVISAT ASAR data to detect oil spills. Several image-processing techniques were used, including calibration and re-projection (Figs. 2 and 3).

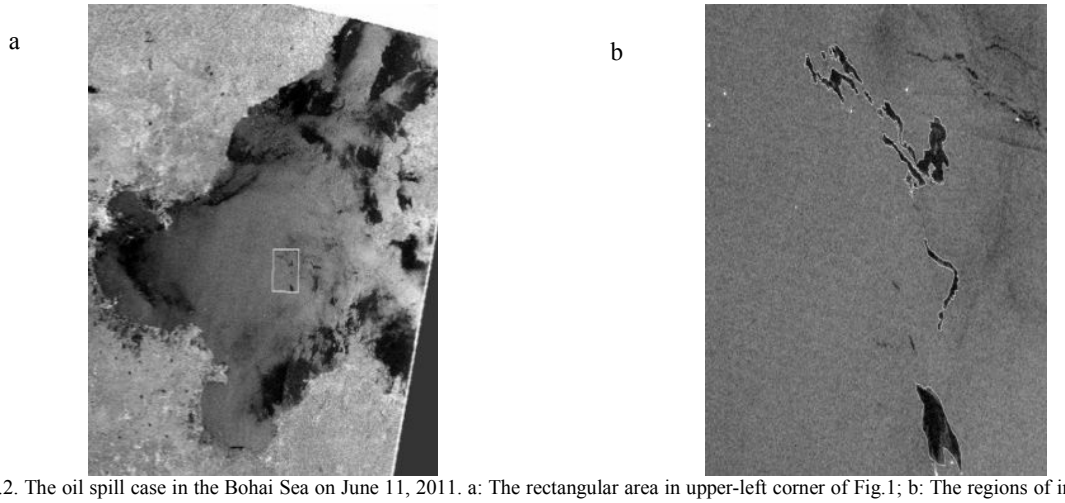

Fig.2. The oil spill case in the Bohai Sea on June 11, 2011. a: The rectangular area in upper-left corner of Fig.1; b: The regions of interest (ROI) is the enlarged area of the small square in Fig.2a. Black spots indicate oil spill patches.

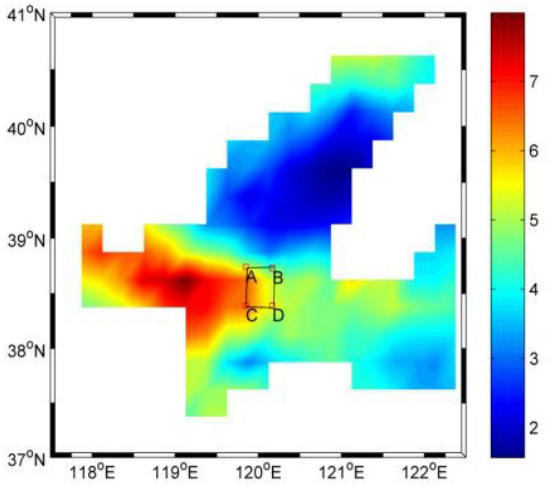

Fig.3. Wind speed retrieved by ASCAT data in oil-spill area of the Bohai Sea on June 11, 2011

The wind fields retrieved by ASCAT data in the oil spill region is shown in Fig.3. We found that the wind speeds in the regions were below 9m/s and the incidence angles of the ROI were within 30°. Therefore, it is capable of discriminating between different surface films with SAR data (Gade and Alpers, 1998).We selected 10 image samples (11-pixel NRCS-averaged as one sample for noise elimination) from the following areas: oil-spill area, clean-sea (nearby oil spill area: the incident angle less than 1 degree area),respectively.

3. Analysis Results

Figure4 shows that the average NRCS of oil spill (data1) is -20.482dB, and that of clean sea (data2) is -12.35 dB. The average NRCS of data1 was 8.132 dB, which is smaller than the average of data2.

Therefore, oil spill could dampen capillary gravity waves and lead to the decreases in NRCS of SAR. Non-Bragg scattering is the dominating mechanism in the areas that covered by oil spill.

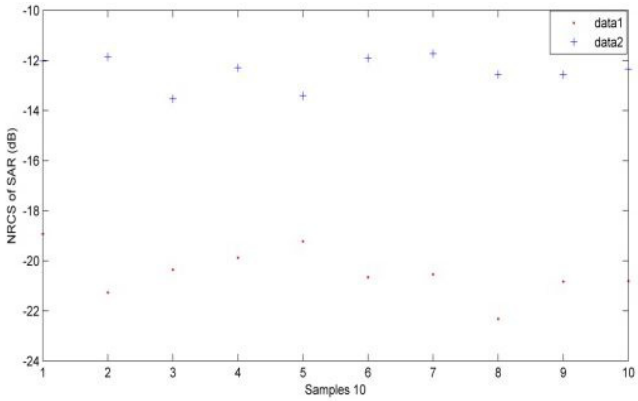

Fig.4. Compare the NRCS of SAR between oil-spill and clean-sea areas on June 11, 2011 in Bohai Sea.

(data1: average NRCS of oil spill samples; data2: average NRCS of clean-sea samples)

3.1. Threshold Determination

Several image-processing techniques were used for Figs.5a, including calibration, re-projection, mean-value filtration (3×3), and then Gama filtration (3×3). Calibration is to get the image of each pixel of NRCS, and then to remove the influence of the incident angle. Re-projection is to remove the mirror effect. Mean-value filtration is to keep the original information of image as much as possible with smooth the image appropriately. Gamma filtration can keep the information at the edge and reduce the speckle noise at the same time (Han et al, 2013). In this study, the adaptive threshold was applied. We determined the mean values of the accident area (oil spill area). Figures 5b show the images of oil spill (the adaptive threshold: -15.9041dB) extracted through the threshold values of NRCS.

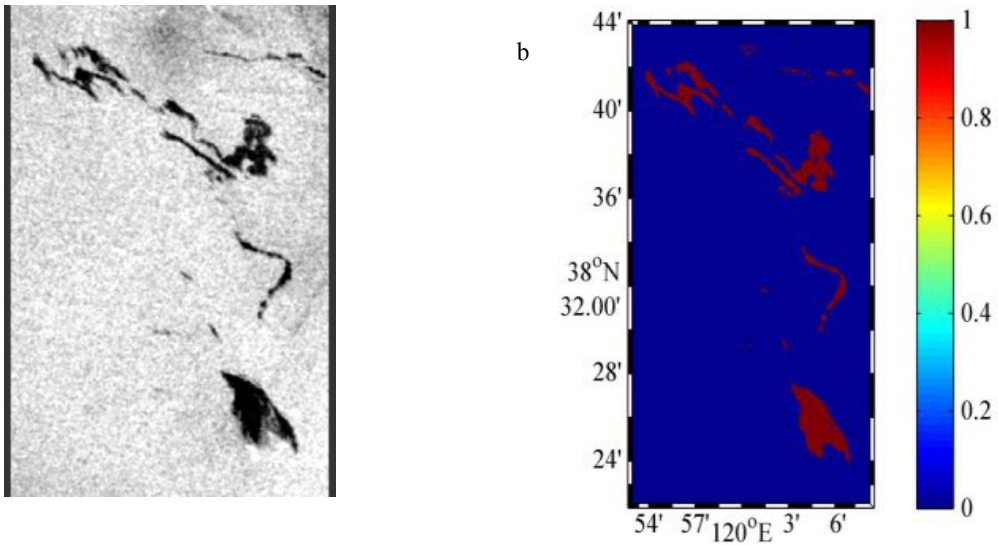

Fig.5. Oil spill distribution section in the Bohai Sea on June 11, 2011 in Fig.2b. a: ROI; b: extracted oil film according to the threshold values

Therefore, how to repair the wind field in the area has become an issue of this study. Although the impact can be negligible for wind field inversion in small-scale oil spill cases for a low-resolution scatterometer, small-scale and mesoscale such cases can have significant impact on local wind field inversion for a high-resolution SAR and

scatterometer.

4. Discussions

4.1. Wind field repair

In this section, we study wind field repair in oil spill areas by CMOD5.n as shown in Figs.2 (rectangular areas). First, radiation on SAR data is calibrated, in which the pixels average of image size for wind speed and direction retrievals is 80×80 at resolution 6×6 km (Figs.6 a rectangle ABDC, the area to be repaired). Second, the wind vectors of the oil spill regions are retrieved and repaired.

Wind speeds inversion was conducted with CMOD5.n, in which the maximum wind velocity for inversion was set to 10m/s. The initial input of wind field of the Bohai Sea is from buoy data that deployed at 38° 2' 1.68" / 119° 51' 3.6" on June 11, 2011. Average wind speed at 10 am was 4.1m/s and average wind direction was 337°. Last, the NRCS-weighted average of adjacent clear-sea areas nearby oil spill scene was used (the incident angle less than 1 degree) for mending the NRCS of oil spill areas. The minimum threshold for oil spill was -9.94dB, while the averages of the clean-sea areas around the two incident scenes were -9.64 and -9.89dB, respectively. The retrieved wind vectors are presented in Figs.6a, corresponding to the regions shown in Figs.2b.

If the threshold of scattering coefficient is smaller than the minimum of the clean-sea water, the average of the clean-sea areas is used to replace those of the scenes. In this study, the average for oil spill scene was -9.64dB, as mentioned in the last paragraph. In addition, Rectangle ABDC in Fig.6 (38.33°–38.65°N, 119.87°–120.10°E) was the ROI of the oil spill area (11.33 km2).

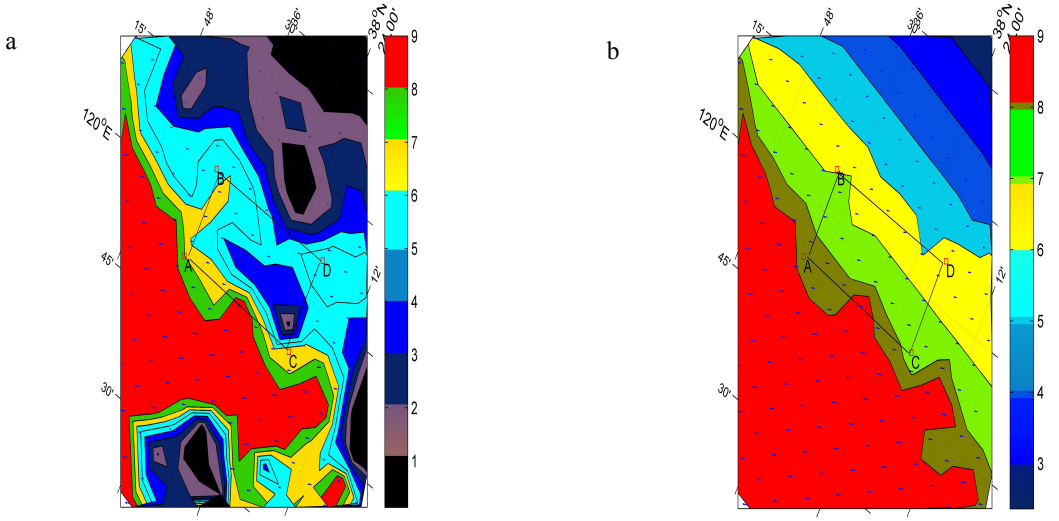

Fig.6. ASAR retrieved wind vectors at sea surface in the oil spill area in the Bohai Sea on June 11, 2011. a: wind field retrieved; b: wind field repaired (Rectangle ABDC in Fig.2b).

4.2. Verification on the wind field repair

As the ASCAT itself contains the signal of oil contamination, we used WRF model to validate the wind field repaired. The configuration of Weather Research and Forecasting (WRF) Model in this study is shown in Table 1.

The initial field and lateral boundary condition were come from the USA National Centres for Environmental Prediction (NCEP) FNL (Final) Operational Global Analysis; and they are on 1°×1° grid in time interval of six hours.

Table1. Configuration of numerical simulation

Parameter	Value
Center coordinates	34.N, 124.E
Grid distance	18km
Map projection	Lambertconformal conic
Grid size	121×121
Vertical levels	27
Time step	90s
Microphysics	WSM 6-class Graupel scheme
Long wave radiation	RRTM scheme
Short wave radiation	Dudhia scheme
PBL physical	YSU scheme
Cumulus Parameterization	Kain-Fritsch (New-Eta) scheme
Initial Time	00Z10June2011/00Z18July2011
End Time	12Z12June2011/12Z20July2011
History interval	60s

The result shows that the difference of wind vector between ASAR retrieved and WRF simulated was within 0.1° and the temporal difference was less than 30 min.

Figure7 shows the wind field simulation by WRF model on the spilled oil scene at 10 am on June 11, 2011 in Bohai Sea (Rectangular ABDC). We used the simulation result to verify the repaired wind field data of the oil spill scene (Fig.6b). In this area, 39 pairs of wind speed and wind direction were compared for the ROI in Fig.6b with those in Fig.7 The RMS, A-error and R-error in wind speed (wind direction) is as small as 0.89 m/s (20.26°), 0.74m/s (19.94°), and -0.02m/s (-0.11°), respectively (Table 2), which is a good result (Fig.8a and 8b).

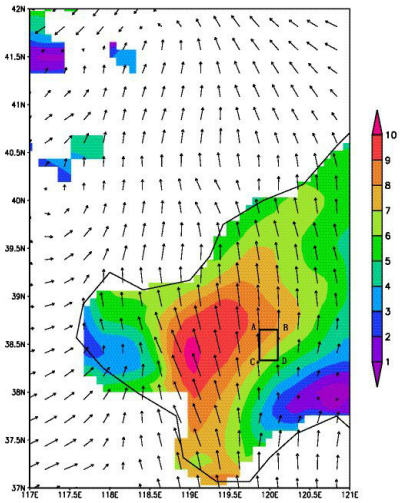

Fig.7. The wind field simulation by WRF model

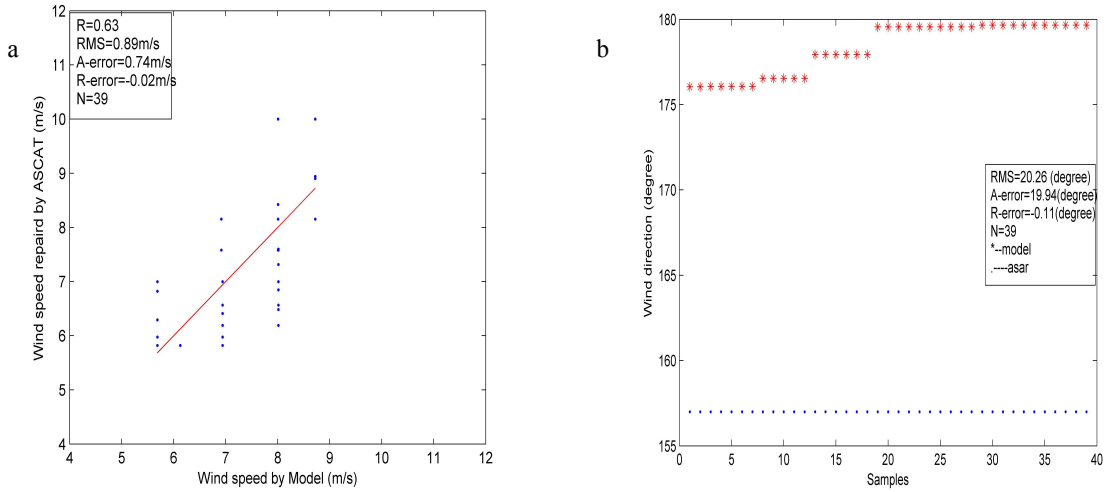

Fig.8. Comparison in wind speed (a) and wind direction (b) for the oil spill case on June 11, 2011 in Bohai Sea between ASAR-restored and WRF-simulated results

Table2. The root means square error (RMS), absolute error (A-error), and relative error (R-error) of oil spill (as shown Fig6b) (in Rectangle ABDC) between WRF model data and SAR data

Date	Number	RMS-V (V_dir)	A-error-V (V_dir)	R-error-V (V_dir)
2011-06-11	39	0.89 m/s (20.26°)	0.74 m/s (19.94°)	-0.02 m/s (-0.11°)

5. Conclusions

In this paper, we use the NRCS image samples of SAR to distinguish between the areas of oil spill and clean sea, and using the adaptive threshold of NRCS to extract oil spill and to repair wind speed. The results obtained are good within the scope of the oil spill (Table2), demonstrating that this method can improve the accuracy of the assessment to the real wind field of an incident area. The attempt provides reference to medium-scale and small-scale wind field repair in oil spill and can contribute to the identification, surface monitoring of oil spills, biogenic slicks etc.

Acknowledgements

Thanks are expressed to the Marine Physics and Remote Sensing Research Laboratory and the First Institute of Oceanography, SOA. This paper is support by the National Natural Science Foundation of China (No.41176160) and 135 program of Chinese Academy of Sciences (Y455011031). Data were provided by the European Space Agency.

References

Brekke C, Solberg A H S. 2005. Oil spill detection by satellite remote sensing. Remote Sensing of Environment, 95, 1-13.

Del Frate F, Petrocchi A, Lichtenegger J, Calabresi G, 2000. Neural networks for oil spill detection using ERS SAR data. IEEE Trans. Geosci. Remote Sens., 38, 2282-2287.

Espedal H A, Wahl T. 1999. Satellite SAR oil spill detection using wind history information. International Journal of Remote Sensing, 20, 49–65.

Espedal H A, Johannessen J A. 2000. Detection of oil spills near offshore installations using synthetic aperture radar (SAR). International Journal of Remote Sensing, 11, 2141-2144.

Feng S Z, Li F Q, Li S Q. 2003. An Introduction to Marine Science.Higher Education Press. Beijing.pp. 242

Fiscella B, Giancaspro A, Nirchio F, Pavese P, Trivero P. 2000. Oil spill detection using marine SAR images. Int. J. Remote Sens., 21,3561-3566.

Gade M Alpers W. 1998.Imaging of biogenic and anthropogenic ocean surface films by the multifrequency/multipolarization SIR-C/X-SAR.

Journal of Geophysical Research, 103,18,851-18,866.
Guo J, Liu X, Xie Q. 2013. Characteristics of the Bohai Sea oil spill and its impact on the Bohai Sea ecosystem. Chinese Science Bulletin, 58, 2276-2281.
Han J Q, Meng J M, Zhao J S. 2013. Feature extraction and its criticality analysis for oil spill detection in synthetic aperture radar images. ActaOceanologicaSinica, 35, 85-93.
Hersbach H. 2010. Comparison of C-band scatterometer CMOD5.N equivalent neutral winds with ECMWF.J. Atmos. Ocean. Technol., 27, 721-736.
Karathanassi V, Topouzelis K, Pavlakis P, Rokos D. 2006. An object-oriented methodology to detect oil spills. International Journal of Remote Sensing, 27, 5235-5251.
Keramitsoglou I, Cartalis C, Kiranoudis C. 2005. Automatic identification of oil spills on satellite images. Environmental Modeling and Software, 21,640-652.
Keramitsoglou I, Cartalis C, Kiranoudis C. 2006. Automatic identification of oil spills on satellite images. Environ. Model.Softw., 21, 640-652.
Li Y, Liang G, Yu S M, Chen P. 2011. Selection of microwave remote sensing data of monitoring of Enteromorphaprolifera disaster. Marine Environmental Science, 30, 739-742.
Migliaccio M, Nunziata F, Gambardella A. 2009. On the co-polarized phase difference for oil spill observation. International Journal of Remote Sensing, 30, 1587-1602.
Quilfen Y, Chapron B, Elfouhaily T, Katsaros K, Tournadre J. 1998. Observation of tropical cyclones by high-resolution scatterometry. J. Geophys. Res., 103(C4):7767-7788
Schuler D L, Lee J S, Hoppel K W. 1993. Polarimetric SAR image signatures of the ocean and Gulf Stream features. IEEE Transactions on Geoscience and Remote Sensing, 31,1210-1221.
Skamarock, W. C, Klemp, J. B. 2008.A time-split nonhydrostatic atmospheric model for weather research and forecasting applications. J. Comput. Phys., 227, 3465–3485.
Solberg A H S, Storvik G, Solberg R, Volden E. 1999. Automatic detection of oil spills in ERS SAR images. IEEE Trans. Geosci. Remote Sens, 37, 1916-1924.
Solberg R, Theophilopoulos N A. 1997. ENVISYS-A solution for automatic oil spill detection in the Mediterranean. Proceedings of 4th Thematic Conference on Remote Sensing for Marine and Coastal Environments, pp. 3-12.
Stoffelen A, Anderson D. 1997.Scatterometer data interpretation: Estimation and validation of the transfer function CMOD4. J. Geophys. Res., 102, 5767-5780.
Topouzelis K, Karthanassi V, Pavlakis P, RokosD. 2003. Oil spill detection: SAR multi-scale segmentation & object features evaluation. In Proceedings of SPIE. Remote Sensing of the Ocean and Sea Ice, 4880, 77-87.
Topouzelis K, Stathakis D, Karathanassi V. 2009. Investigation of genetic algorithms contribution to feature selection for oil spill detection. International Journal of Remote Sensing, 30, 611-625.
Zhang B, Perrie W, Vachon P W, Li X F, Pichel W G, Guo J, He Y J. 2012. Ocean vector winds retrieval from C-B and fully polarimetric SAR measurements. IEEE Transactions on Geoscience and Remote Sensing, 50, 4252-4261.